Dynamic effect of overhangs and islands at the depinning transition in two-dimensional magnets

N. J. Zhou and B. Zheng*

Zhejiang Institute of Modern Physics, Zhejiang University, Hangzhou 310027, People's Republic of China and Asia Pacific Center for Theoretical Physics, POSTECH, Pohang 790-784, South Korea

(Received 5 July 2010; revised manuscript received 5 September 2010; published 29 September 2010)

With the Monte Carlo methods, we systematically investigate the short-time dynamics of domain-wall motion in the two-dimensional random-field Ising model with a driving field (DRFIM). We accurately determine the depinning transition field and critical exponents. Through two different definitions of the domain interface, we examine the dynamics of overhangs and islands. At the depinning transition, the dynamic effect of overhangs and islands reaches maximum. We argue that this should be an important mechanism leading the DRFIM model to a different universality class from the Edwards-Wilkinson equation with quenched disorder.

DOI: 10.1103/PhysRevE.82.031139 PACS number(s): 64.60.Ht

I. INTRODUCTION

In the past years, much effort of physicists has been devoted to domain-wall dynamics in magnetic devices, nanomaterials, thin films, semiconductors, contact lines, and fluid invasion in porous media [1–6]. In particular, quenched randomness in ferroic materials, e.g., ultrathin ferromagnetic and ferroelectric films, fundamentally affects the response to an external field [7–10]. From a pragmatic point of view, understanding the controlled movement of domain walls plays an important role in developing new classes of potential nonvolatile storage-class memories [8,11,12]. From a purely theoretical point of view, it is also essential for understanding nonequilibrium dynamics in disordered media [13–16]. For a dc (direct current) driving field, H, the domain-wall motion exhibits a depinning transition at zero temperature. The depinning field, H_c, separates the regimes of static pinning ($H<H_c$) and friction-limited viscous slide ($H>H_c$) [17–20]. At low, but nonzero, temperatures, the sharp depinning transition is softened and a thermally activated creep state appears [21,22]. For an ac (alternative current) driving field, $H(t)=H_0\, exp(i2\pi ft)$, and at a nonzero temperature, the domain-wall motion exhibits different states and dynamic phase transitions, which can be classified in the so-called Cole-Cole diagrams [23–25].

Current theoretical approaches to domain-wall dynamics in ultrathin films are typically based on the Edwards-Wilkinson equation with quenched disorder (QEW) [14,18,26,27]. This equation is a phenomenological model, and detailed microscopic structures and interactions of real materials are not concerned. Additionally, a self-inconsistence is puzzling at the depinning transition, especially for the roughness exponent ζ [28–30]. To understand the domain-wall motion at a microscopic level, one needs lattice models based on microscopic structures and interactions [17,21,31]. The random-field Ising model with a driving field (DRFIM) is a candidate, at least to capture robust features of the domain-wall motion, although it does not include all interactions in real materials.

As an interface propagates, overhangs and islands may occur. Such a phenomenon is observed in many experiments for magnetic materials [32,33]. In the QEW equation, an interface is described by a single-valued elastic string, and overhangs and islands are not taken into account [22,34,35]. However, the anomalous roughness exponent ($\zeta \neq 1$) has led one to conjecture that a one-dimensional string necessarily develops overhangs and islands [28]. In the DRFIM model, overhangs and islands are naturally created; thus, the domain wall is not single-valued and one-dimensional [36–38]. Numerical simulations of the DRFIM model show that characteristics of the domain-wall motion may depend on overhangs and islands [16,39]. In the literatures, however, the dynamics of overhangs and islands is rarely referred, and its dynamic effect on the depinning transition is not identified.

In the past years much progress has been achieved in critical dynamics far from equilibrium [40–43]. Although the spatial correlation length is still short in the beginning of the time evolution, the short-time dynamic scaling form is induced by the divergent correlating time around a continuous phase transition. Based on the *short-time* dynamic scaling form, new methods for the determination of both dynamic and static critical exponents have been developed [43,44]. Since the measurements are carried out in the short-time regime, one does not suffer from critical slowing down. Recent activities include various applications and developments such as theoretical and numerical studies of the Josephson-junction arrays and aging phenomena [45–49]. A kind of domain-wall roughening process at order-disorder phase transitions has also been revealed [50–52]. Very recently, the short-time behavior of the domain-wall relaxation around the depinning transition is noted in simulations and experiments [14,15,53].

In a recent article [16], based on the short-time dynamic approach, the domain-wall dynamics of a disordered magnetic system driven by a constant field H is investigated with the DRFIM model, in comparison with the QEW equation and experiments. The depinning transition at zero temperature is of second order, and its ordered parameter is the interface velocity. The transition field, static and dynamic exponents, and local and global roughness exponents are accurately determined for the DRFIM model. The results indicate that the DRFIM model may not belong to the universality class of the QEW equation [16], in contrast to the usual assumption [35,37].

However, it is unknown what mechanism leads to the difference between the DRFIM model and QEW equation. The

*Corresponding author; zheng@zimp.zju.edu.cn

fluctuation and correlation of the interface velocity and, especially, the dynamics of overhangs and islands are not touched at all. Due to the existence of overhangs and islands, the definition of the domain interface is theoretically not unique, and comparison with experiments remains ambiguous. The purpose of this paper is to provide a comprehensive understanding of the depinning transition in the DRFIM model. We emphasize that the dynamics of overhangs and islands plays a key role. In Sec. II, the model and scaling analysis are described. In Sec. III, numerical results are presented. Sec. IV includes the conclusions.

II. MODEL AND SCALING ANALYSIS

A. Model

The random-field Ising model is defined by the Hamiltonian

$$\mathcal{H} = -J\sum_{\langle ij\rangle} S_i S_j - H\sum_i S_i - \sum_i h_i S_i, \tag{1}$$

where $S_i = \pm 1$ is the Ising spin of the two-dimensional square lattice. The random field h_i is uniformly distributed within an interval $[-\Delta, \Delta]$ and H is a homogeneous driving field. Following Refs. [16,17], we fix $\Delta = 1.5J$ and set $J=1$. For comparison, $\Delta = 0$ is also simulated. A Gaussian distribution of the random field h_i leads to similar results, but it is technically more complicated. Therefore, the results of the uniform distribution of h_i are presented in this paper. Our simulations are performed at zero temperature with lattice sizes $L=128$, 256, 512, and 1024 up to $t_{max}=2000$, with total samples of 10 000, 40 000, 50 000, and 30 000, respectively. Simulations of different L confirm that our results do not suffer from finite-size effects. Errors are estimated by dividing the samples into three or four subgroups. If the fluctuation of the curve in the time direction is comparable with or larger than the statistical error, it will be taken into account.

The initial state is such a state that spins are positive in the sublattice on the left side and negative on the right side. We set the x axis in the direction perpendicular to the perfect domain wall. Antiperiodic and periodic boundary conditions are used in x and y directions, respectively. To eliminate the pinning effect irrelevant for disorder, we rotate the square lattice such that the initial domain wall orients in the (11) direction of the square lattice, as shown in Refs. [16,17,21,39]. After preparing the initial state, we *randomly* select a spin and flip it if the total energy decreases after flipping. A Monte Carlo time step is defined by L^2 single-spin selects. As time evolves, the domain wall moves and roughens.

We should emphasize that our simulations of the DRFIM model are carried out at zero temperature and with not so strong disorder ($\Delta = 1.5$), therefore the bulk does *not* evolve. Overhangs and islands are naturally created during the time evolution but only *by the domain wall*. Therefore, it makes sense to define the domain wall as an interface, the so-called domain interface. Due to the existence of overhangs and islands, however, there may be different ways to define the domain interface. In this paper, two typical definitions of the domain interface are concerned to investigate the dynamics of overhangs and islands and to compare with the QEW equation and experiments. We first study the definition commonly used in the literatures, i.e., the one defined by the magnetization [16,17,21]. Denoting a spin at site (x,y) by $S_{xy}(t)$, we introduce a *line* magnetization,

$$m(y,t) = \frac{1}{L}\left[\sum_{x=1}^{L} S_{xy}(t)\right]. \tag{2}$$

The height function of the domain interface is then defined as

$$h_m(y,t) = \frac{L}{2}[m(y,t)+1]. \tag{3}$$

The subscript m indicates that it is defined by the line magnetization. Thus, the roughness function is introduced to depict the roughening of the domain interface,

$$\omega_m^{(2)}(t) = \langle h_m(y,t)^2\rangle - \langle h_m(y,t)\rangle^2, \tag{4}$$

where $\langle\cdots\rangle$ includes the statistical average and average over y. A more informative quantity is the height correlation function [34],

$$C_m(r,t) = \langle [h_m(y+r,t) - h_m(y,t)]^2\rangle. \tag{5}$$

It describes both the spatial correlation of the height function in the y direction and the growth of the domain interface in the x direction. To *independently* estimate the dynamic exponent z, we introduce an observable

$$F_m(t) = [M^{(2)}(t) - M(t)^2]/\omega_m^2(t). \tag{6}$$

Here, $M(t)$ is the *global* magnetization and $M^{(2)}(t)$ is its second moment. In fact, $F_m(t)$ is nothing but the ratio of the planar susceptibility and line susceptibility.

On the other hand, the local interface velocity is defined as the time derivative of the height function [17],

$$v_m(y,t) = \frac{dh_m(y,t)}{dt}. \tag{7}$$

The average velocity of the domain interface is then obtained,

$$v_M(t) = v_m(t) = \langle v_m(y,t)\rangle. \tag{8}$$

Here, we use the subscript M to emphasize that $v_M(t)$ is the global average velocity. In fact, $v_M(t)$ is the order parameter of the depinning phase transition. The local and global fluctuations of the local interface velocity, $v_m^{(2)}(t)$ and $v_M^{(2)}(t)$, are interesting observables,

$$v_m^{(2)}(t) = \langle v_m(y,t)^2\rangle - v_M(t)^2, \tag{9}$$

$$v_M^{(2)}(t) = \left\langle \left[\frac{1}{L}\sum_{y=1}^{L} v_m(y,t)\right]^2\right\rangle - v_M(t)^2. \tag{10}$$

In Eq. (10), $\langle\cdots\rangle$ only includes the statistical average. We note that $v_m^{(2)}(t)$ describes the fluctuation of the interface velocity in the x direction, while $v_M^{(2)}(t)$ also includes the correlation of the interface velocity in the y direction.

In the definition of the height function in Eq. (3), overhangs and islands look formally suppressed. However, they

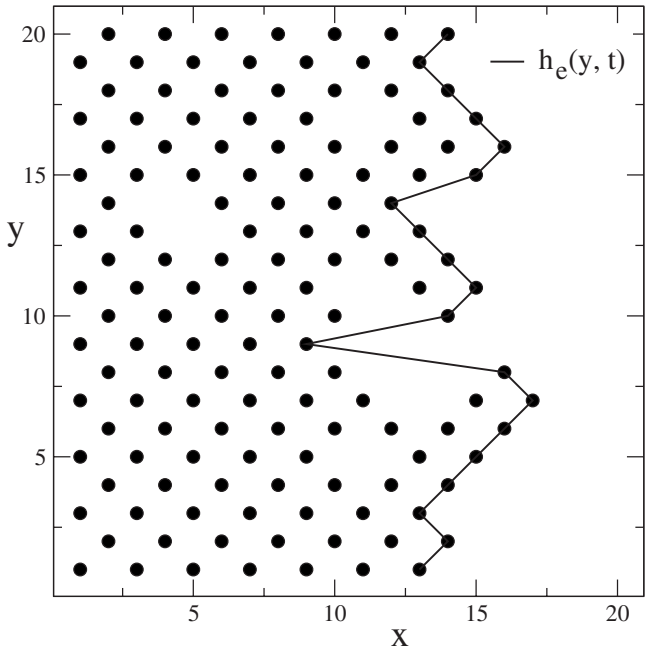

FIG. 1. Height function $h_e(y,t)$ is defined as the envelop of the positive spins.

do affect the dynamic evolution of the spin configuration and contribute to the interface propagation and growth [16]. Due to the existence of overhangs and islands, however, the definition of the domain interface is not unique. Whether different definitions lead to the same results and how to compare with the QEW equation and experiments remain ambiguous. For example, another definition of the height function can be introduced by the *envelop* of the positive spins, as shown in Fig. 1. In other words, we define the height function $h_e(y,t)$ as the largest x coordinate of the positive spins with the fixed y coordinate and at the time t. This definition is closer to the experiments with imaging technique [2,32,33].

With $h_e(y,t)$, one can derive the local interface velocity $v_e(y,t)$. Similar to Eqs. (4)–(10), the average velocity $v_E(t)$, the roughness function $\omega_e^2(t)$, the function $F_e(t)$, the height correlation function $C_e(r,t)$, and the local and global fluctuations of the velocity, $v_e^{(2)}(t)$ and $v_E^{(2)}(t)$, can be calculated. In the definition of the height function with the envelop, the dynamic effect of overhangs and islands is *maximally* taken into account. In contrast to it, the height function defined with the magnetization includes only a minimal contribution of overhangs and islands.

To reveal the dynamic characteristics of overhangs and island, therefore, we may introduce the overhang height function $\delta h(y,t)$ and local overhang velocity $\delta v(y,t)$,

$$\delta h(y,t) = h_e(y,t) - h_m(y,t), \tag{11}$$

$$\delta v(y,t) = v_e(y,t) - v_m(y,t). \tag{12}$$

Then, the average overhang velocity is

$$\delta v(t) = v_E(t) - v_M(t), \tag{13}$$

and it is related to the average overhang size by

$$\delta h(t) = \int_0^t \delta v(t')dt'. \tag{14}$$

Similar to Eqs. (4), (9), and (10), the roughness function of overhangs and islands, $\delta h^{(2)}(t)$, and the local and global fluctuations of the overhang velocity, $\delta v_l^{(2)}(t)$ and $\delta v_G^{(2)}(t)$, can be defined,

$$\delta h^{(2)}(t) = \langle [\delta h(y,t)]^2 \rangle - [\delta h(t)]^2, \tag{15}$$

$$\delta v_l^{(2)}(t) = \langle [\delta v(y,t)]^2 \rangle - [\delta v(t)]^2, \tag{16}$$

$$\delta v_G^{(2)}(t) = \left\langle \left[\frac{1}{L} \sum_{y=1}^{L} \delta v(y,t) \right]^2 \right\rangle - [\delta v(t)]^2. \tag{17}$$

To measure the dynamic exponent independently, we can construct a function $F_\delta(t)$ in a similar form of Eq. (6).

B. Scaling analysis

Since the depinning transition is a second-order phase transition, the dynamic evolution of the order parameter $v_M(t)$ should obey the dynamic scaling theory supported by the renormalization-group calculations [40,43,44]. For a finite lattice size L and assuming a nonequilibrium correlation length $\xi \sim t^{1/z}$, scaling arguments lead to a dynamic scaling form for the order parameter [40,43,44],

$$v_M(t,\tau,L) = b^{-\beta/\nu} G(b^{-z}t, b^{1/\nu}\tau, b^{-1}L). \tag{18}$$

Here, b is an arbitrary rescaling factor, β and ν are the static exponents, z is the dynamic exponent, and $\tau = (H - H_c)/H_c$. Setting $b \sim \xi(t) \sim t^{1/z}$, the dynamic scaling form is rewritten as

$$v_M(t,\tau,L) = t^{-\beta/\nu z} G(1, t^{1/\nu z}\tau, t^{-1/z}L). \tag{19}$$

In the short-time regime, i.e., the regime with $\xi(t) \sim t^{1/z} \ll L$, the finite-size effect is negligibly small,

$$v_M(t,\tau) = t^{-\beta/\nu z} G(t^{1/\nu z}\tau). \tag{20}$$

Therefore, at the transition point $\tau = 0$, a power-law behavior is obtained,

$$v_M(t) = t^{-\beta/\nu z}. \tag{21}$$

With Eq. (20), the critical field H_c may be located by searching for the best power-law behavior of $v_M(t,\tau)$ [43,44]. The critical exponent $\beta/\nu z$ is then estimated from Eq. (21). The critical exponent $1/\nu z$ can be obtained from the time derivative of $v_M(t,\tau)$, calculated according to Eq. (20) [16].

In general, even at the transition point, the roughness function $\omega_m^2(t)$, the height correlation function $C_m(r,t)$, and the global fluctuation $v_M^{(2)}(t)$ of the interface velocity in Eqs. (4), (5), and (10) may not obey a perfect power-law behavior in early times. Due to the random updating scheme in numerical simulations, the domain interface and its velocity also roughen *even without disorder* ($\Delta = 0$), although no overhangs and islands are generated. This may induce corrections to scaling. To capture the dynamic effect of disorder, we introduce the pure roughness function $D\omega_m^2(t)$, the pure height correlation function $DC_m(r,t)$, and the pure global

fluctuation $Dv_M^{(2)}(t)$ by subtracting the contributions of $\Delta=0$, $\omega_{m,b}^2(t)$, $C_{m,b}(r,t)$, and $v_{M,b}^{(2)}(t)$, respectively. For a sufficiently large lattice and at the transition point, we should observe standard power-law scaling behaviors [16,20,34,51],

$$D\omega_m^2(t) \sim t^{2\zeta/z} \tag{22}$$

and

$$DC_m(r,t) \sim \begin{cases} t^{2(\zeta-\zeta_{loc})/z} r^{2\zeta_{loc}} & \text{if } r \ll \xi(t) \ll L \\ t^{2\zeta/z} & \text{if } 0 \ll \xi(t) \ll r. \end{cases} \tag{23}$$

Here, $\xi(t) \sim t^{1/z}$, ζ is the global roughness exponent, and ζ_{loc} is the local one. Finally, the dynamic exponent z is independently determined by

$$F_m(t) \sim t^{1/z}/L. \tag{24}$$

Compared with the velocity itself, the global and local fluctuations of the velocity exhibit more complicated dynamic behaviors. In fact, there are two intrinsic length scales at the depinning transition, the correlation length $\xi(t) \sim t^{1/z}$ in the y direction and the characteristic length of roughening in the x direction, $l(t) \sim t^{\zeta/z}$, defined in Eq. (22). It only happens that $l(t)$ is irrelevant for the average velocity $v_M(t)$. In general, therefore, the pure global fluctuation of the interface velocity should obey the scaling form [43,44]

$$Dv_M^{(2)}(t) = t^{-2\beta/\nu z} F(\xi(t)/L, l(t)/\xi(t)). \tag{25}$$

For a sufficiently large lattice, finite-size scaling analysis leads to [43,44]

$$Dv_M^{(2)}(t) \sim (\xi(t)/L)^d, \tag{26}$$

where $d=1$ is the spatial dimension of the domain interface. Our numerical simulations show that the dependence of $Dv_M^{(2)}(t)$ on $l(t)/\xi(t)$ takes also a power law. Therefore,

$$Dv_M^{(2)}(t) \sim t^{[1-2\beta/\nu+\lambda_M(\zeta-1)]/z}/L, \tag{27}$$

where λ_M is an exponent, reflecting the dynamic effect of the roughness of the domain interface. Similarly, the local fluctuation of the interface velocity corresponds to $d=0$,

$$v_m^{(2)}(t) \sim t^{[-2\beta/\nu+\lambda_m(\zeta-1)]/z}. \tag{28}$$

In fact, our numerical simulations yield $\lambda_M \approx 2$ and $\lambda_m \approx 3$. For the standard order-disorder phase transition, such terms described by λ_M and λ_m do not exist since the roughness exponent is $\zeta=1$ [51,52]. This is a difference between the depinning transition and the standard order-disorder phase transition.

In the above scaling analysis, we do not consider the possible length scale induced by overhangs and islands. Actually, the height function of the domain interface defined with the magnetization in Eq. (3) does not include the length scale of overhangs and islands. The dynamic effect of overhangs and islands in this case comes only through the dynamic evolution of the multiple domain walls. On the other hand, in our numerical simulations, we do observe the dynamic scaling behavior described in Eqs. (18)–(28). Therefore, we assume that for the domain interface defined with the magnetization, overhangs and islands may only influence the critical exponents.

It is, however, very different for the domain interface defined with the envelop of the positive spins, where the height function as shown in Fig. 1 does explicitly include the length scale of overhangs and islands. Due to this extra length scale, in principle, the dynamic scaling forms described in Eqs. (18)–(28) are not valid. In the short-time regime, however, we numerically detect an effective critical point, at which the dynamic scaling forms in Eqs. (18)–(24) hold approximately. Thus, we could also determine the effective critical exponents. However, the global and local fluctuations of the interface velocity are complicated and do not obey the power-law scaling forms in Eqs. (27) and (28) even at the effective critical point.

To deeply understand the dynamic effect of overhangs and islands, we may independently examine the dynamics of overhangs and islands. Similar to the determination of the critical field H_c from Eq. (20), one can locate the critical field H_c by searching for the best power-law behavior of the overhang velocity $\delta v(t,H)$. At the critical point H_c, however, the overhang velocity $\delta v(t)$ *increases* with time, different from the interface velocity $v(t)$. For example, we may write

$$\delta v/v \sim t^{\theta}. \tag{29}$$

Here, θ is estimated to be about 0.5 in our numerical simulations. In general, $\delta h(y,t)$ and $\delta v(y,t)$ are dynamic variables independent of $h_m(y,t)$ and $v_m(y,t)$, and one needs another set of critical exponents to describe their dynamic behaviors. Similar to $D\omega^{(2)}(t)$ in Eq. (22), the pure roughness function of overhangs and islands obeys [16,51,52]

$$D\delta h^{(2)}(t) \sim t^{2\zeta_\delta/z_\delta}, \tag{30}$$

where ζ_δ and z_δ are the roughness exponent and dynamic exponent of overhangs and islands, respectively. The dynamic exponent z_δ can be independently determined from

$$F_\delta(t) \sim t^{1/z_\delta}/L. \tag{31}$$

Since the overhang velocity $\delta v(y,t)$ does not show correlation in the y direction, we assume that both the local and global fluctuations of the overhang velocity, $\delta v_l^{(2)}(t)$ and $\delta v_G^{(2)}(t)$, defined in Eqs. (16) and (17) obey

$$\delta v^{(2)}(t) \sim t^{2\alpha}. \tag{32}$$

On the other hand, the global fluctuation $\delta v_G^{(2)} \sim L^{-1}$, while the local one $\delta v_l^{(2)}$ and the roughness function $\delta h^{(2)}(t)$ are L independent.

III. NUMERICAL SIMULATIONS

In Ref. [16], the dynamic scaling behaviors from Eq. (20) up to Eq. (24) have been carefully examined for the domain interface defined with the magnetization in the DRFIM model. The relevant critical exponents are accurately determined and are summarized in Table I, in comparison with those of the QEW equation. Due to the extra length scale induced by overhangs and islands, our first task in this paper is to investigate whether and to what extent these dynamic scaling forms hold also for the domain interface defined with the envelop of the positive spins.

TABLE I. Depinning transition field and critical exponents obtained for the DRFIM model are compared with those for the QEW equation in Refs. [14,18,19,35,54]. The exponents β, ν, z, ζ, and ζ_{loc} for the domain interface defined with the magnetization are taken from Ref. [16].

		QEW	Magnetization	Envelop	Overhang
$v(t)$	H_c		1.2933(2)	1.2913(4)	1.294(1)
	β	0.33(2); 0.33	0.295(3)	0.278(4)	
	ν	1.29(5); 1.33; 1.33(1)	1.02(2)	1.02(4)	$\gg 1$
	z	1.5; 1.53	1.33(1)	1.28(1)	1.11(1)
	θ				0.50(2)
$\omega^2(t)$	ζ	1.26(1); 1.25; 1.24	1.14(1)	1.14(1)	1.16(2)
$C(r,t)$	ζ	1.23(1); 1.25	1.13(1)	1.14(1)	
	ζ_{loc}	0.98; 0.92	0.735(8)	0.569(6)	
$v_M^{(2)}(t)$	λ		2.04(5)		
$v_m^{(2)}(t)$			3.06(3)		
$\delta v_G^{(2)}(t)$	α				0.501(3)
$\delta v_l^{(2)}(t)$					0.488(4)

In Fig. 2(a), the average interface velocity $v_E(t,\tau)$ is displayed for different driving field H. It drops rapidly down for smaller H while approaches a constant for larger H. Due to the length scale of overhangs and islands, $v_E(t,\tau)$ does not exhibit a power-law scaling behavior at the transition field $H_c=1.2933$ located from $v_M(t,\tau)$. By searching for the best power-law behavior of $v_E(t,\tau)$, however, one could detect an effective transition field $H_c=1.2913(4)$, which is slightly smaller than $H_c=1.2933(2)$ obtained from $v_M(t,\tau)$. Although the difference between the effective transition field and the real one looks small, it is not a statistical error. We believe that this difference is induced by the length scale of overhangs and islands at the nonstationary stage of the dynamic evolution. Anyway, the critical exponent $\beta/\nu z=0.210(2)$ is obtained from the slope of the curve at H_c, according to Eq. (21). In a similar way, we measure $1/\nu z=0.76(3)$, $2\zeta/z=1.78(1)$, and $1/z=0.778(7)$ based on Eqs. (20), (22), and (24), respectively [16]. We then calculate the effective critical exponents $\beta=0.278(4)$, $\nu=1.02(4)$, $z=1.28(1)$, and $\zeta=1.14(1)$.

In Fig. 2(b), the pure height correlation function $DC_e(r,t)$ is displayed as a function of r at H_c for different time t. According to Eq. (23), the critical exponent $2\zeta_{loc}=1.13(2)$ is derived from the slope of the curve at a large time $t=2000$. To fully confirm the scaling form of $DC_e(r,t)$ in Eq. (23), for example, we fix $t'=1024$ and rescale r of another t to $(t'/t)^{1/z}r$ and $DC_e(r,t)$ to $(t'/t)^{2\zeta/z}DC_e(r,t)$. As shown in Fig. 2(b), data of different t nicely collapse to the curve of $t'=1024$ with $\zeta=1.14$ and $z=1.28$ as input. Hence, the scaling form is validated. In experiments, the critical exponent ζ_{loc} is usually measured from the power-law behavior $DC_e(r,t)\sim r^{2\zeta_{loc}}$ at a large t. Indeed, this power-law behavior of $DC_e(r,t)$ is much cleaner than that of $DC_m(r,t)$, as shown in the inset. Plotting $DC_e(r,t)$ as a function of t for different

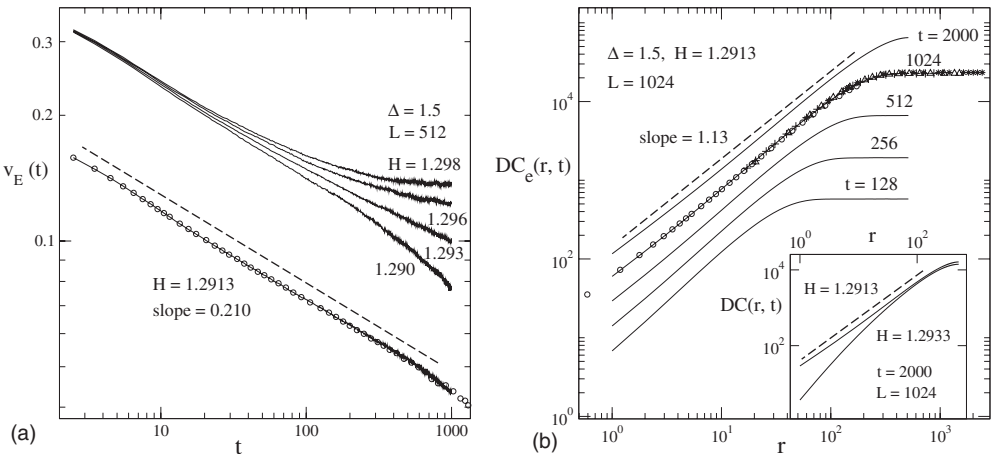

FIG. 2. (a) Interface velocity $v_E(t,\tau)$ is plotted with solid lines for different driving fields H with $L=512$ on a log-log scale. For clarity, the curve of $H=1.2913$ is shifted down. For comparison, the curve with $L=1024$ is shown with open circles. (b) The pure height correlation function $DC_e(r,t)$ is displayed at $H_c=1.2913$. According to Eq. (26), data collapse is demonstrated. Stars, triangles, pluses, and circles correspond to $t=128$, 256, 512, and 2000, respectively. In the inset, $DC(r,t)$ defined with the envelop (upper) and with the magnetization (lower) are shown at $t=2000$. In both (a) and (b), dashed lines show power-law fits.

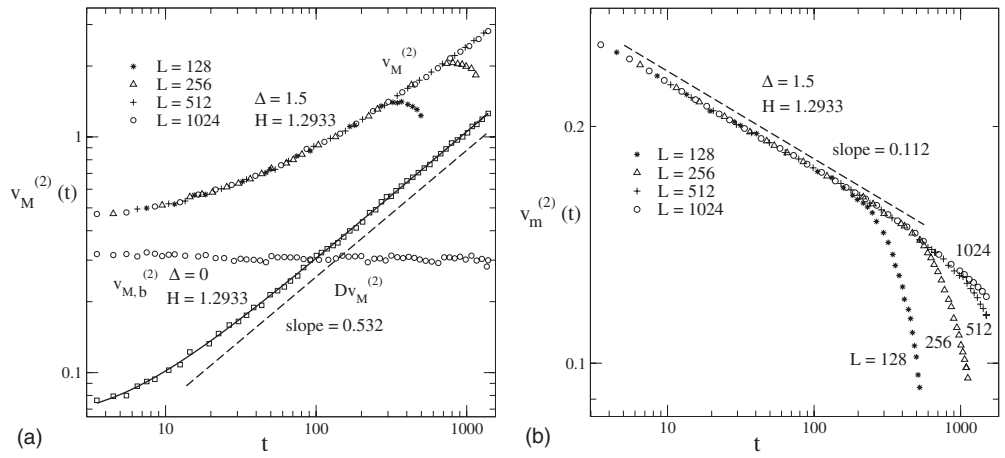

FIG. 3. In (a) and (b), the global and local fluctuations of the interface velocity are displayed at $H_c=1.2933$ for different L on a log-log scale. Dashed lines show power-law fits, and the solid line represents a power-law fit with correction. In (a), the pure global fluctuation function $Dv_M^{(2)}(t)$ is shown for $L=1024$ with squares. All the curves have been rescaled by a factor L.

r, we measure $2\zeta/z=1.78(1)$ and $2(\zeta-\zeta_{loc})/z=0.890(5)$ based on Eq. (23). With the dynamic exponent $z=1.28(1)$ as input, we may calculate ζ and ζ_{loc}. The global roughness exponent $\zeta=1.14(1)$ is the same as that obtained from the roughness function, and the local roughness exponent $\zeta_{loc}=0.569(6)$ is consistent with $\zeta_{loc}=0.565(10)$ measured directly in Fig. 2(b).

All the measurements of the effective transition field and critical exponents are summarized in Table I, in comparison with the transition field and critical exponents for the domain interface defined with the magnetization and for the QEW equation. For the domain interface defined with the magnetization, the exponents β, z and ζ of the DRFIM model differ from those of the QEW equation by about 10%, and especially, the difference of ν and ζ_{loc} between two models reaches nearly 30% [16]. For the domain interface defined with the envelop, the difference is even larger. For the exponent ζ_{loc}, for example, the difference between two models is about 45%. These results suggest that it is mainly the overhangs and islands that induce the difference between the DRFIM model and QEW equation. Our numerical simulations based on the short-time dynamic approach indicate that the DRFIM model and QEW equation are not in a same universality class [16,36]. Although real materials may include more complicated interactions than the DRFIM model, experimental measurements of the local roughness exponent of the domain interface support $\zeta_{loc}<1$. For $T>0$ and $0<H<H_c$, for example, it is reported that $\zeta_{loc}=0.7(1)$ and 0.69(7) in the experiments with ultrathin Pt/Co/Pt films [7,2] and $\zeta_{loc}=0.78(1)$ with $Co_{28}Pt_{72}$ alloy films [33].

In the stationary state, the depinning transition should be uniquely defined. Therefore, the transition field located from the short-time dynamic behavior of $v_E(t,\tau)$ is an effective one. In other words, $v_E(t,\tau)$ is not a "good" order parameter in rigorous sense, although it is closer to and helps us understand the experiments with imaging technique [2,32,33]. To demonstrate the difference between the domain interfaces defined with the magnetization and envelop, we may consider the fluctuation of the interface velocity. In Fig. 3(a), the global fluctuations of the interface velocity, $v_M^{(2)}(t)$ and $v_{M,b}^{(2)}(t)$ for $\Delta=1.5$ and 0, and the pure global fluctuation $Dv_M^{(2)}(t)=v_M^{(2)}(t)-v_{M,b}^{(2)}(t)$ are displayed. Obviously $Dv_M^{(2)}(t)$ shows a cleaner power-law behavior than $v_M^{(2)}(t)$ does due to the subtraction of $v_{M,b}^{(2)}(t)$. The slope of the curve $Dv_M^{(2)}(t)$ is 0.532(5). Including a power-law correction, e.g., $Dv^{(2)}(t)\sim t^b(1+c/t)$, may improve the fitting to the numerical data, and the resulting exponent is consistent with 0.532(5) within errors. According to Eq. (27), one can calculate the exponent $\lambda_M=2.04(5)$ from $[1-2\beta/\nu+\lambda_M(\zeta-1)]/z=0.532$. In Fig. 3(b), the local fluctuation $v_m^{(2)}(t)$ is plotted, and the slope of the curve is 0.112(3). According to Eq. (28), $\lambda_m=3.06(3)$ can be derived from $[-2\beta/\nu+\lambda_m(\zeta-1)]/z=-0.112$. To study possible finite-size effects, $v_M^{(2)}(t)$ and $v_m^{(2)}(t)$ computed with different lattice sizes at $H_c=1.2933$ are also shown in Fig. 3. All the curves in Fig. 3(a) are rescaled by a factor L based on Eq. (27). As it can be seen in the figure, the finite-size effect can be easily controlled; i.e., it drops rapidly as L increases. This is a merit of the short-time dynamic approach [16,42–44].

However, both $Dv_E^{(2)}(t)$ and $v_e^{(2)}(t)$ do not exhibit a power-law behavior either at $H_c=1.2913$ or 1.2933. In other words, they do not obey the scaling forms in Eqs. (27) and (28). Additionally, $v_e(y,t)$ does not show a standard correlation in the y direction. In fact, the domain interface defined with the envelop may be considered as adding overhangs and islands to the domain interface defined with the magnetization. To understand the domain interface defined with the envelop, we may alternatively investigate the dynamics of overhangs and islands. In the inset of Fig. 4(a), we present the overhang velocity $\delta v(t)$ for different driving field H. Different from the velocity $v_M(t)$ and $v_E(t)$ of the domain interface, $\delta v(t)$ drops rapidly down for both smaller and larger driving field H and reaches maximum at the transition point H_c, which is estimated to be between 1.29 and 1.30. In order to determine the transition field more accurately, we calculate the overhang size $\delta h(t,H)$ as a function of the external field H at $t=1000$. As shown in Fig. 4(a), the maximum of $\delta h(H)$ yields $H_c=1.294(1)$, in good agreement with the transition field $H_c=1.2933(2)$ estimated from $v_M(t)$. The dynamic effect of overhangs and islands is the most prominent at the

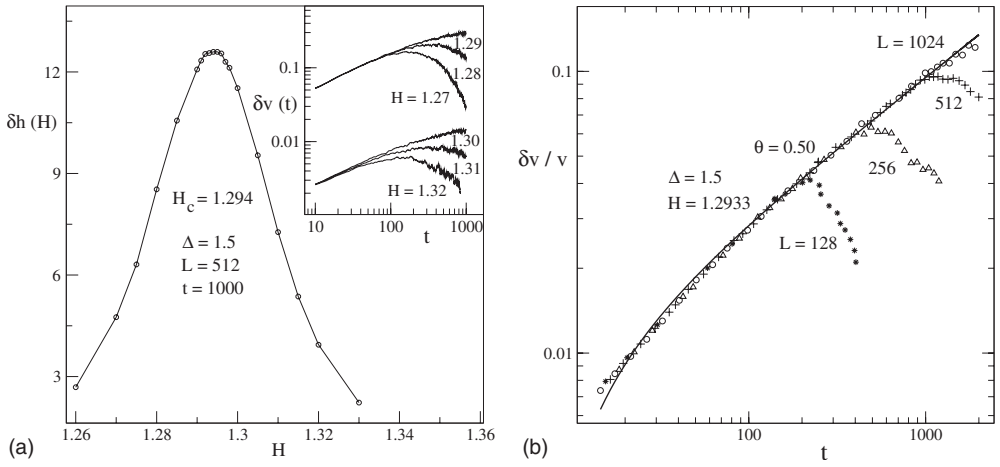

FIG. 4. (a) The overhang size $\delta h(t,H)$ is plotted as a function of the driving field H at $t=1000$. In the inset, the overhang velocity $\delta v(t)$ is shown for different H on a log-log scale. For clarity, the curves for $H=1.29$, 1.28, and 1.27 are shifted up. (b) $\delta v/v$ is displayed at $H_c=1.2933$ for different L on a log-log scale. The solid line represents a power-law fit with correction.

depinning transition point. In Fig. 4(b), $\delta v/v$ is plotted at $H=1.2933$ with different lattice size L. The finite-size effect is negligible for $L=1024$ up to $t=2000$. According to Eq. (29), $\theta=0.50(2)$ is obtained with a power-law fit for $t>100$, and a power-law correction improves the fitting to the numerical data.

To determine the dynamic exponent z_δ, we plot the function $F_\delta(t)$ at $H_c=1.2933$ in Fig. 5(a). The slope of the curve with $L=512$ is 090(1), and it yields $z_\delta=1.11(1)$. A power-law correction may improve the fitting to the numerical data. Collapse of the curves with $L=256$ and 512 indicates the L dependence $F_\delta(t)\sim 1/L$. In Fig. 5(b), the roughness functions $\delta h^{(2)}(t)$ and $\delta h_b^{(2)}(t)$ for $\Delta=1.5$ and 0 and the pure roughness function $D\delta h^{(2)}(t)$ are displayed at $H=1.2933$. Obviously, $D\delta h^{(2)}(t)$ exhibits a cleaner power-law behavior than $\delta h^{(2)}(t)$. The slop of the curve is 2.10(3), and it leads to $\zeta_\delta=1.16(2)$, close to $\zeta=1.14$ for the domain interface. With a correction to scaling, i.e., $D\delta h^{(2)}(t)\sim t^{2\zeta_\delta/z_\delta}(1+c/t^2)$, the fitting to numerical data is extended. Since both the overhang size and velocity reach a maximum at the transition field H_c, the standard exponent ν is not defined. In other words, $\partial_H \delta v(t,H)$ is close to zero at H_c, and effectively, $\nu_\delta \gg 1$.

Finally, we consider the local and global fluctuations of the overhang velocity. In Fig. 6, the local fluctuation $\delta v_l^{(2)}(t)$ is plotted at $H=1.2933$. By the definition, the local fluctuation can also be calculated with $\delta v_l^{(2)}(t)=v_e^{(2)}(t)-v_m^{(2)}(t)-2\Delta(t)$ and $\Delta(t)=\langle v_m(y,t)\delta v(y,t)\rangle - v_M(t)\delta v(t)$. Hence, $v_e^{(2)}(t)-v_m^{(2)}(t)$ is plotted for comparison. The result indicates that $\delta v_l^{(2)}(t)\approx v_e^{(2)}(t)-v_m^{(2)}(t)$, i.e., $\Delta(t)\approx 0$. According to Eq. (32), a direct measurement from the slope of the curve gives $2\alpha=0.972(4)$. A power-law correction to scaling yields a similar result of $2\alpha=0.976$. The global fluctuation $\delta v_G^{(2)}(t)$ and $v_E^{(2)}(t)-v_M^{(2)}(t)$ are also plotted in Fig. 6. Both of them are rescaled by a factor of $L/4$ because of the finite-size dependence of L^{-1}. Overlapping of these two curves is observed and it yields $\Delta(t)\approx 0$, too. The exponent $2\alpha=1.002(5)$ is determined from the slope, in agreement with that measured from the local fluctuation of the velocity. Actually, our numerical simulations show that $\delta v_l^{(2)}(t)\approx L\delta v_G^{(2)}(t)$. In Fig. 6, it is only for clarity that $\delta v_G^{(2)}(t)$ is rescaled by a factor of $L/4$

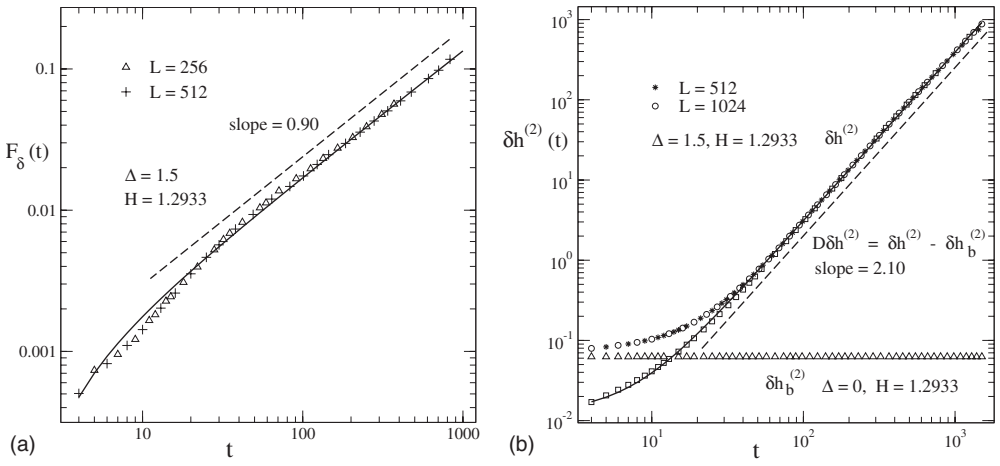

FIG. 5. (a) $F_\delta(t)$ is plotted at $H_c=1.2933$. The curve of $L=256$ has been rescaled by a factor 1/2 according to Eq. (31). (b) The roughness function and pure roughness function of overhangs and islands are displayed at $H_c=1.2933$. In both (a) and (b), dashed lines show power-law fits, while solid lines are for power-law fits with correction.

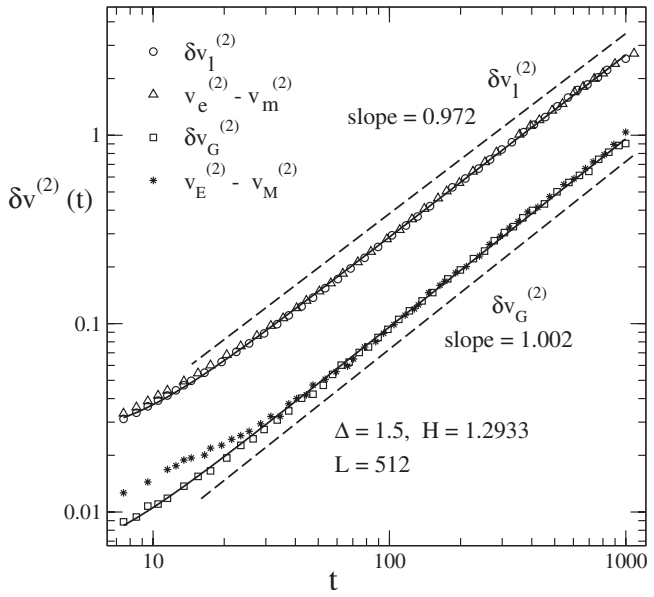

FIG. 6. Local and global fluctuations of the overhang velocity, $\delta v_l^{(2)}$ and $\delta v_G^{(2)}$, are plotted on a log-log scale. For comparison, $v_e^{(2)}-v_m^{(2)}$ and $v_E^{(2)}-v_M^{(2)}$ are also displayed. To show the finite-size dependence, the global quantities are rescaled by a factor of $L/4$. Dashed lines show power-law fits, while solid lines are for power-law fits with correction.

rather than L. The result $\Delta(t)\approx 0$ indicates that $v_m(y,t)$ and $\delta v(y,t)$ are not correlated, and therefore, another set of critical exponents is needed for describing the dynamic behavior of overhangs and islands.

The fact that both $\delta v_l^{(2)}(t)$ and $\delta v_G^{(2)}(t)$ are governed by the same exponent $\alpha\approx 0.5$ indicates that the overhang velocity $\delta v(y,t)$ is not correlated in the y direction, although the overhang size $\delta h(y,t)$ does. If we consider $\delta v(y,t)$ as "a height function," its roughening process described by $\delta v_l^{(2)}(t)$ belongs to the universality class of random depositions. Why does such a phenomenon occur? For example, $h_e(y+1,t)$ may suddenly produce an overhang at $h_e(y,t)$ and induce a rapid increase of the overhang velocity $\delta v(y,t)$. However, this is not correlated with $\delta v(y+1,t)$. For the domain interface defined with the envelop, $v_e(y,t)$ is also not correlated in the y direction, since $v_e(y,t)=v_m(y,t)+\delta v(y,t)$, and $\delta v(y,t)$ dominates at larger t. At the transition field H_c, our numerical simulations show that $v_e^{(2)}(t)\approx v_m^{(2)}(t)+\delta v_l^{(2)}(t)$ and $v_E^{(2)}(t)\approx v_M^{(2)}(t)+\delta v_G^{(2)}(t)$. On the other hand, $\delta v_l^{(2)}(t)$ and $\delta v_G^{(2)}(t)$ exhibit different power-law behaviors from $v_m^{(2)}(t)$ and $v_M^{(2)}(t)$, respectively. Therefore, $v_e^{(2)}(t)$ and $v_E^{(2)}(t)$ do not obey a simple power law. For large t, however, $\delta v_l^{(2)}(t)$ and $\delta v_G^{(2)}(t)$ dominate the dynamic behaviors of $v_e^{(2)}(t)$ and $v_E^{(2)}(t)$.

IV. SUMMARY

Based on the short-time dynamic approach, we have systematically investigated the domain-wall dynamics of the DRFIM model at the depinning transition. Through two different definitions of the domain interface, we examine the dynamics of overhangs and islands. All the critical exponents and transition field (or effective ones) for the domain interface and for overhangs and islands are summarized in Table I.

For the domain interface defined with the envelop, we observe that the dynamic scaling behaviors in Eqs. (20)–(24) hold approximately at an effective transition field $H_c=1.2913$, slightly below $H_c=1.2933$ determined from the interface velocity defined with the magnetization. The difference of the critical exponents between the DRFIM model and QEW equation becomes lager for the domain interface defined with the envelop, especially for the local roughness exponent ζ_{loc}. These results indicate that the DRFIM model and QEW equation may be not in the same universality class. We argue that it is mainly the overhangs and islands that induce the difference between the DRFIM model and QEW equation. Experiments report the local roughness exponent $\zeta_{loc}<1$ [2,7,33]. Although it is rather tedious and difficult, it may be interesting in the future to perform large-scale simulations at the steady state and determine the critical point and exponents from the finite-size scaling behavior. This may provide a further judgment on the universality classes of the DRFIM model and QEW equation.

The global and local fluctuations of the interface velocity defined with the magnetization exhibit the power-law scaling behaviors described by the exponents λ_M and λ_m in Eqs. (27) and (28), while those defined with the envelop do not. It indicates that the interface velocity defined with the envelop is not a good order parameter of the depinning transition, although it is closer to and helps us understand experiments with imaging techniques. In fact, $v_e(y,t)$ is also not correlated in the y direction. It should be interesting to measure the fluctuation and correlation of the interface velocity in experiments.

At the depinning transition, the dynamics effect of overhangs and islands reaches maximum. The observables of overhangs and islands do obey the dynamic scaling forms in Eqs. (29)–(32), similar to those for the domain interface. However, another set of critical exponents should be introduced since $v_m(y,t)$ and $\delta v(y,t)$ are not correlated. Different from the interface velocity, the overhang velocity increases with time. The dynamic exponent $z_\delta=1.11(1)$ for overhangs and islands is smaller than $z_\delta=1.33(1)$ for the domain interface, while the roughness exponent is about the same. In particular, the overhang velocity $\delta v(y,t)$ does not show correlation in the y direction, although the overhang size $\delta h(y,t)$ does. Considering $\delta v(y,t)$ as a height function, its roughening process belongs to the universality class of random depositions. Since $h_e(y,t)=h_m(y,t)+\delta h(y,t)$, the domain interface defined with the envelop can be mostly understood by adding overhangs and islands to that defined with the magnetization.

ACKNOWLEDGMENTS

This work was supported in part by NNSF of China under Grant Nos. 10875102 and 11075137, Fundamental Research Funds for Central Universities, Zhejiang Provincial Natural Science Foundation of China under Grant No. Z6090130, and the JRG program of APCTP.

[1] S. J. He, G. L. M. K. S. Kahanda, and P. Z. Wong, Phys. Rev. Lett. **69**, 3731 (1992).
[2] S. Lemerle, J. Ferré, C. Chappert, V. Mathet, T. Giamarchi, and P. Le Doussal, Phys. Rev. Lett. **80**, 849 (1998).
[3] T. Ono, H. Miyajima, K. Shigeto, K. Mibu, N. Hosoito, and T. Shinjo, Science **284**, 468 (1999).
[4] S. Moulinet, A. Rosso, W. Krauth, and E. Rolley, Phys. Rev. E **69**, 035103(R) (2004).
[5] M. Yamanouchi, J. Ieda, F. Matsukura, S. E. Barnes, S. Maekawa, and H. Ohno, Science **317**, 1726 (2007).
[6] M. Y. Im, L. Bocklage, P. Fischer, and G. Meier, Phys. Rev. Lett. **102**, 147204 (2009).
[7] P. J. Metaxas, J. P. Jamet, A. Mougin, M. Cormier, J. Ferré, V. Baltz, B. Rodmacq, B. Dieny, and R. L. Stamps, Phys. Rev. Lett. **99**, 217208 (2007).
[8] Y. H. Shin, I. Grinberg, I. W. Chen, and A. M. Rappe, Nature (London) **449**, 881 (2007).
[9] A. Dourlat, V. Jeudy, A. Lemaître, and C. Gourdon, Phys. Rev. B **78**, 161303(R) (2008).
[10] K. J. Kim, J. C. Lee, S. M. Ahn, K. S. Lee, C. W. Lee, Y. J. Cho, S. Seo, K. H. Shin, S. B. Choe, and H. W. Lee, Nature (London) **458**, 740 (2009).
[11] M. Hayashi, L. Thomas, R. Moriya, C. Rettner, and S. S. P. Parkin, Science **320**, 209 (2008).
[12] S. S. P. Parkin, M. Hayashi, and L. Thomas, Science **320**, 190 (2008).
[13] A. B. Kolton, A. Rosso, and T. Giamarchi, Phys. Rev. Lett. **95**, 180604 (2005).
[14] A. B. Kolton, A. Rosso, E. V. Albano, and T. Giamarchi, Phys. Rev. B **74**, 140201(R) (2006).
[15] A. B. Kolton, G. Schehr, and P. Le Doussal, Phys. Rev. Lett. **103**, 160602 (2009).
[16] N. J. Zhou, B. Zheng, and Y. Y. He, Phys. Rev. B **80**, 134425 (2009).
[17] U. Nowak and K. D. Usadel, Europhys. Lett. **44**, 634 (1998).
[18] O. Duemmer and W. Krauth, Phys. Rev. E **71**, 061601 (2005).
[19] A. B. Kolton, A. Rosso, T. Giamarchi, and W. Krauth, Phys. Rev. Lett. **97**, 057001 (2006).
[20] B. Bakó, D. Weygand, M. Samaras, W. Hoffelner, and M. Zaiser, Phys. Rev. B **78**, 144104 (2008).
[21] L. Roters, S. Lübeck, and K. D. Usadel, Phys. Rev. E **63**, 026113 (2001).
[22] A. B. Kolton, A. Rosso, and T. Giamarchi, Phys. Rev. Lett. **94**, 047002 (2005).
[23] T. Braun, W. Kleemann, J. Dec, and P. A. Thomas, Phys. Rev. Lett. **94**, 117601 (2005).
[24] W. Kleemann, J. Rhensius, O. Petracic, J. Ferré, J. P. Jamet, and H. Bernas, Phys. Rev. Lett. **99**, 097203 (2007).
[25] W. Jeżewski, W. Kuczyński, and J. Hoffmann, Phys. Rev. B **77**, 094101 (2008).
[26] T. Nattermann, S. Stepanow, L. H. Tang, and H. Leschhorn, J. Phys. II **2**, 1483 (1992).
[27] S. Bustingorry, A. B. Kolton, and T. Giamarchi, EPL **81**, 26005 (2008).
[28] A. Rosso and W. Krauth, Phys. Rev. Lett. **87**, 187002 (2001).
[29] H. Leschhorn and L. H. Tang, Phys. Rev. Lett. **70**, 2973 (1993).
[30] H. J. Jensen, J. Phys. A **28**, 1861 (1995).
[31] F. Colaiori, G. Durin, and S. Zapperi, Phys. Rev. Lett. **97**, 257203 (2006).
[32] K. S. Lee, C. W. Lee, Y. J. Cho, S. Seo, D. H. Kim, and S. B. Choe, IEEE Trans. Magn. **45**, 2548 (2009).
[33] M. Jost, J. Heimel, and T. Kleinefeld, Phys. Rev. B **57**, 5316 (1998).
[34] M. Jost and K. D. Usadel, Phys. Rev. B **54**, 9314 (1996).
[35] A. Rosso, A. K. Hartmann, and W. Krauth, Phys. Rev. E **67**, 021602 (2003).
[36] J. S. Urbach, R. C. Madison, and J. T. Markert, Phys. Rev. Lett. **75**, 276 (1995).
[37] Luis A. Nunes Amaral, A. L. Barabási, H. A. Makse, and H. E. Stanley, Phys. Rev. E **52**, 4087 (1995).
[38] L. Roters, A. Hucht, S. Lübeck, U. Nowak, and K. D. Usade, *Structure and Dynamics of Heterogeneous Systems* (World Scientific, Singapore, 2000).
[39] L. Roters, A. Hucht, S. Lübeck, U. Nowak, and K. D. Usadel, Phys. Rev. E **60**, 5202 (1999).
[40] H. K. Janssen, B. Schaub, and B. Schmittmann, Z. Phys. B: Condens. Matter **73**, 539 (1989).
[41] D. A. Huse, Phys. Rev. B **40**, 304 (1989).
[42] B. Zheng, M. Schulz, and S. Trimper, Phys. Rev. Lett. **82**, 1891 (1999).
[43] B. Zheng, Int. J. Mod. Phys. B **12**, 1419 (1998).
[44] H. J. Luo, L. Schülke, and B. Zheng, Phys. Rev. Lett. **81**, 180 (1998).
[45] E. Granato and D. Dominguez, Phys. Rev. B **71**, 094521 (2005).
[46] P. Calabrese and A. Gambassi, J. Phys. A **38**, R133 (2005).
[47] X. W. Lei and B. Zheng, Phys. Rev. E **75**, 040104 (2007).
[48] S. Z. Lin and B. Zheng, Phys. Rev. E **78**, 011127 (2008).
[49] H. K. Lee and Y. Okabe, Phys. Rev. E **71**, 015102(R) (2005).
[50] N. J. Zhou and B. Zheng, EPL **78**, 56001 (2007).
[51] N. J. Zhou and B. Zheng, Phys. Rev. E **77**, 051104 (2008).
[52] Y. Y. He, B. Zheng, and N. J. Zhou, Phys. Rev. E **79**, 021107 (2009).
[53] G. Rodríguez-Rodríguez, A. Pérez-Junquera, M. Vélez, J. V. Anguita, J. I. Martín, H. Rubio, and J. M. Alameda, J. Phys. D **40**, 3051 (2007).
[54] J. M. López and M. A. Rodríguez, J. Phys. I **7**, 1191 (1997).